doi:10.6041/j.issn.1000-1298.2026.02.040

Hybrid Controller for Steady Speed of Agricultural Machinery on Slopes

WU Caicong[1,2]　XU Haisong[1,2]　GAO Xingyu[1,2]

(1. *College of Information and Electrical Engineering*, *China Agricultural University*, *Beijing* 100083, *China*
2. *Key Laboratory of Agricultural Machinery Monitoring and Big Data Application*, *Ministry of Agriculture and Rural Affairs*, *Beijing* 100083, *China*)

Abstract: Steady speed control of agricultural machinery can improve operating quality and efficiency. To address the impact of farmland slope variations on the speed stability of unmanned operation agricultural machinery, a hybrid control method was proposed. This method included a hybrid controller composed of a slope-based controller and a proportional-integral-derivative (PID) controller. The speed of agricultural machinery was influenced by longitudinal forces, which were divided into two parts: one part was slope-related forces and conventional resistance, and the other was hard-to-estimate forces, such as sliding friction. For the first part, a slope-based controller was designed; for the second part, a PID controller was implemented. By combining these two controllers, the system can dynamically adjust the throttle opening and the brake master cylinder pressure, ensuring steady speed travel on sloping farmland. Simulation tests at a target speed of 7 km/h demonstrated that the proposed controller maintained a stable speed, achieving a root mean square error of 0.13 km/h and a mean absolute percentage error of 1.6%. Field tests on a practical experimental platform validated the method's effectiveness, with results showing consistent control performance across varying slope conditions. The proposed controller demonstrated superior control performance. Experimental data verified that this method can achieve precise control of the agricultural machinery's movement speed, meeting the stability requirements for agricultural operations.

Key words: farmland slope; PID controller; steady speed control; agricultural machinery; unmanned operation

CLC number: S220　**Document code**: A　**Article ID**: 1000-1298(2026)02-0416-11　**OSID**:

0 Introduction

Unmanned agricultural machinery was a key development direction for modern agriculture[1-2]. On sloping farmland, terrain variations can cause speed fluctuations of agricultural machinery, affecting the uniformity and precision of operations such as seeding and spraying[3-6]. Therefore, achieving steady speed control of unmanned agricultural machines on sloping farmland was critical to improving the quality of agricultural production.

To maintain a steady speed, the vehicle's speed can be determined using feedback from the wheel speedometer or positioning system. Based on the current speed, a method to adjust and achieve the target speed can then be applied[7-10]. For instance, WANG et al.[7] designed a longitudinal speed control algorithm based on the cascade of two PID controllers. The outer loop generates the desired pedal position based on the tractor's speed and the inner loop produces the electrohydraulic valve voltage value based on the pedal position through a cascade control mechanism. OLEIWI et al.[9] developed a nonlinear PID control algorithm optimized using the Aquila optimization method, which enhanced the system's robustness by fine-tuning the PID parameters, achieving precise speed tracking and effectively suppressing disturbances.

However, when the agricultural machine's load changed or the terrain slope changed, large fluctuations

Received date: 2024-09-11　Accepted date: 2025-02-11

Foundation item: National Key Research and Development Program of China(2023YFE0208200)

First author: WU Caicong (1975—), professor, Ph.D. E-mail: wucc@cau.edu.cn

in speed may occur due to the lack of necessary external information. Therefore, researchers introduced external information to achieve steady-speed driving in complex scenarios[11-12]. For example, ZHAO et al.[11] designed a work-condition-based cooperative control strategy for cruise control, dynamically adjusted the throttle opening and variable pump displacement based on traction resistance and other working conditions, achieving stable speed control for tractors during flat land operation. WU et al.[12] developed a tractor speed stabilization algorithm using a digital elevation model. By extracting the slope information of the working path ahead from the field DEM based on the tractor's real-time location, the algorithm calculated the compensation for the target speed ahead of the tractor, thereby realizing longitudinal speed control.

In order to achieve low-cost and efficient steady-speed driving for agricultural machines on sloped terrain, a hybrid controller composed of a slope-based controller and a proportional-integral-derivative (PID) controller was proposed and the construction method for the slope-based controller was provided. The slope-based controller effectively overcame the impact of the gravitational component, while the PID controller compensated for the effects of other resistances, dynamically adjusting the output to achieve steady-speed driving for agricultural machines on sloped terrain.

1　Materials and methods

1.1　Longitudinal forces analysis

The longitudinal dynamics model of a vehicle characterized the movement characteristics of agricultural machinery by analyzing the forces acting on it under different terrain conditions[13]. Considering the main forces acting on agricultural machinery during longitudinal movement, including the gravitational component, driving force, braking force and operational resistance (covering rolling resistance, mechanical resistance and etc., but excluding the gravitational component). The force analysis diagram of the vehicle was shown in Fig. 1.

Assuming that the mass of the agricultural machinery was constant, the gravitational component acting on the machinery was related to its pitch angle, which was determined by the slope of the farmland.

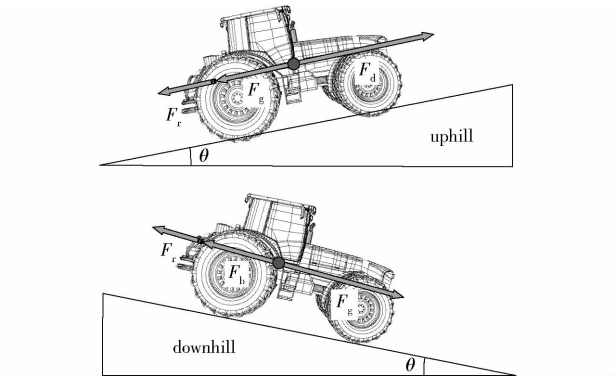

Fig. 1　Schematic of longitudinal forces on agricultural machinery on sloped terrain

The relationship between the gravitational component and the ground slope can be expressed as following

$$F_g = f_g(\theta) \tag{1}$$

where　F_g——gravitational component, N

θ——ground slope, %

The operational resistance was the reaction force generated by the environment or the machinery's own conditions during the operation of the system. For a specific agricultural machinery, the operational resistance fluctuated around an average value under specific working conditions and can be expressed by formula (2).

$$F_r = F_0 + \varepsilon \tag{2}$$

where　F_r——total operational resistance, N

F_0——conventional resistance, N

ε——smaller disturbance term that cannot be accurately estimated, N

During the operation of agricultural machinery, it was necessary to reasonably choose the timing for driving and braking. When the machinery was going uphill ($\theta > 0$) the driving force needs to overcome the gravitational component and the operational resistance. The relationship of forces was given by formula (3).

$$F_d = F_g + F_r \tag{3}$$

where　F_d——driving force, N

When going downhill ($\theta < 0$), a critical slope θ_1 was defined as the slope where the agricultural machinery remains stationary relying solely on conventional resistance F_0 (without extra driving or braking force); downhill conditions were divided into two categories based on this critical slope: when $\theta_1 < \theta$, the gravitational component was approximately smaller than the operational resistance, so driving force was still needed, with the force relationship following formula (4).

$$F_d + F_g = F_r \tag{4}$$

when $\theta_1 > \theta$, the gravitational component was approximately larger than the operational resistance, so braking force was required, with the force relationship following formula (5).

$$F_g = F_b + F_r \tag{5}$$

where F_b—— braking force, N

1.2 Hybrid controller design

The forces affecting the agricultural machinery's longitudinal motion primarily included gravitational components and operational resistance, and they can be divided into two categories based on whether they can be accurately estimated. One category covered estimable forces. These forces included the slope-related gravitational component, which can be calculated using terrain slope and machinery mass, and the conventional resistance. The conventional resistance was a stable average value of operational resistance under specific working conditions and can be determined through pre-testing. The other category consisted of non-estimable forces. These forces were a subpart of operational resistance that fluctuated randomly, such as rolling friction from tire deformation or irregular ground friction, and they cannot be precisely predicted due to variable external factors.

θ was difficult to measure directly. Since most tractors adopted a rigid chassis combined with a fixed or simply swinging axle structure, the vehicle pitch angle can be used as an approximate substitute for the ground slope information. Moreover, most unmanned agricultural machinery was equipped with an inertial navigation system; therefore, the vehicle pitch angle can be measured by the on-board attitude sensor of the inertial navigation system, and then the ground slope information can be obtained indirectly.

The driving force was related to the output power. The throttle opening determined the fuel supply and the fuel supply in turn affected the driving force[14]. Therefore, the relationship between the pitch angle and throttle opening can be established through measurement.

For the gravitational component related to the slope and the conventional resistance within the operational resistance, driving force was required when $\theta > \theta_1$. In this case the relationship between the throttle opening and the vehicle pitch angle was shown in formula (6).

$$\alpha_e(\gamma) = \begin{cases} f(F_g + F_0) & (\gamma \geqslant \gamma_1) \\ 0 & (\gamma < \gamma_1) \end{cases} \tag{6}$$

where γ——vehicle pitch angle, (°)

γ_1——vehicle pitch angle when the vehicle was on the ground with ground slope θ_1, (°)

$\alpha_e(\gamma)$——throttle opening corresponding to pitch angle γ under estimable conditions, %

When $\theta > \theta_1$ braking force needed to be output, and the pressure of the brake master cylinder determined the effect of the braking system, thereby affecting the magnitude of the braking force[15]. In this case the relationship between the brake master cylinder pressure and the vehicle pitch angle was shown in formula (7).

$$p_e(\gamma) = \begin{cases} 0 & (\gamma \geqslant \gamma_1) \\ g(F_g - F_r) & (\gamma < \gamma_1) \end{cases} \tag{7}$$

where $p_e(\gamma)$——brake master cylinder pressure corresponding to pitch angle γ under estimable conditions, MPa

The forces that cannot be accurately estimated due to other factors, such as the rolling resistance caused by tire deformation and friction when the wheels were in contact with the road during the agricultural machinery's driving process, would also affect the machinery's movement. The PID controller was simple in form, suitable for low-computing environments and easy to understand and master as a low-cost constrained predictive controller[16]. Therefore, the PID controller was used to continuously adjust the throttle opening or brake master cylinder pressure to respond in real-time to unpredictable changes in resistance[16].

The input to the PID controller was the speed error, which was the difference between the actual speed and the target speed. This speed error was given by formula (8).

$$e_k = v_k - v_t \tag{8}$$

where e_k——speed error in the k-th cycle, km/h

v_k——average speed in the k-th cycle, km/h

v_t——target speed, km/h

Since the throttle opening and brake master cylinder pressure were two different types of data, a PID controller for throttle opening and a PID controller

for brake master cylinder pressure were constructed. For the speed errors required by different PID controllers, the speed error in each cycle was classified into two types based on the vehicle's speed.

$$e_{\alpha,k}(v)=\begin{cases}e_k & (v\leqslant v_t)\\ 0 & (v>v_t)\end{cases} \tag{9}$$

where v——vehicle's current speed, km/h

$e_{\alpha,k}$——speed error input to the throttle opening PID controller, km/h

$$e_{p,k}(v)=\begin{cases}0 & (v\leqslant v_t)\\ e_k & (v>v_t)\end{cases} \tag{10}$$

where $e_{p,k}$——speed error input to the brake master cylinder pressure PID controller, km/h

The PID controller for the throttle opening was given by formula (11).

$$\alpha_{ne}(v,n)=\begin{cases}K_{\alpha p}e_{\alpha,n}+K_{\alpha i}\sum_{k=0}^{n}e_{\alpha,k}+K_{\alpha d}(e_{\alpha,n}-e_{\alpha,n-1}) & (v\leqslant v_t)\\ 0 & (v>v_t)\end{cases} \tag{11}$$

where $K_{\alpha p}$——proportional coefficient of the throttle opening PID controller

$K_{\alpha i}$——derivative coefficient of the throttle opening PID controller

$K_{\alpha d}$——integral coefficient of the throttle opening PID controller

$\alpha_{ne}(v,n)$——throttle opening corresponding to vehicle's speed v under cannot estimable conditions in the n-th cycle, %

The PID controller for the brake master cylinder pressure was given by formula (12).

$$p_{ne}(v,n)=\begin{cases}0 & (v\leqslant v_t)\\ K_{pp}e_{p,n}+K_{pi}\sum_{k=0}^{n}e_{p,k}+K_{pd}(e_{p,n}-e_{p,n-1}) & (v>v_t)\end{cases} \tag{12}$$

where K_{pp}——proportional coefficient of the brake master cylinder pressure PID controller

K_{pi}——derivative coefficient of the brake master cylinder pressure PID controller

K_{pd}——integral coefficient of the brake master cylinder pressure PID controller

$p_{ne}(v,n)$——brake master cylinder pressure corresponding to vehicle's speed v under cannot estimable conditions in the n-th cycle, MPa

The total output of the throttle opening was given by formula (13).

$$\alpha(\gamma,v,n)=\begin{cases}\alpha_e(\gamma)+\alpha_{ne}(v,n) & (v\leqslant v_t)\\ 0 & (v>v_t)\end{cases} \tag{13}$$

The total output of the brake master cylinder pressure was given by formula (14).

$$p(\gamma,v,n)=\begin{cases}0 & (v\leqslant v_t)\\ p_e(\gamma)+p_{ne}(v,n) & (v>v_t)\end{cases} \tag{14}$$

1.3 CarSim and simulink joint simulation

The development of simulation technology provided powerful tools for studying speed control[17-18]. CarSim and Simulink were two widely used simulation platforms[19]. CarSim provided detailed vehicle and road physical simulation models[20-21], while Simulink was used to implement and debug controllers. These simulation tools offered critical technical support for studying steady driving of agricultural machinery on complex terrains. This study conducted joint simulations based on the CarSim and Simulink platforms. Through joint simulation, it was possible to monitor the operating conditions of agricultural machinery in real time under various slope conditions and evaluate the performance of the controller.

To simulate the impact of slope changes on the agricultural machinery's movement, a sloping terrain model with a piecewise linear relationship between slope and horizontal distance was established, as shown in formula (15).

$$y'=\begin{cases}\frac{x}{r}m & (0\leqslant x<r)\\ \left(2-\frac{x}{r}\right)m & (r\leqslant x<3r)\\ \left(\frac{x}{r}-4\right)m & (3r\leqslant x\leqslant 4r)\end{cases} \tag{15}$$

where m——maximum slope, %

x——horizontal distance along the side of the terrain, m

y'——slope, %

r——horizontal length where the slope increased to the maximum or decreased from the maximum, m

Formula (15) divided slope variation into four horizontal distance stages: the slope rised linearly to maximum m ($0 \leqslant x < r$), dropped to 0 ($r \leqslant x < 2r$), decreased to minimum $-m$ ($2r \leqslant x < 3r$), and rebounded to 0. This stage-based variation covered both uphill and downhill scenarios. As shown in Fig. 2, the slope firstly increased linearly and then decreased gradually with the change in horizontal distance.

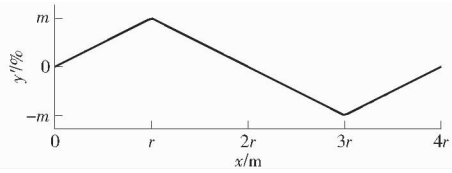

Fig. 2 Curve of test road gradient

Further, using formula (15), the relationship between longitudinal distance and horizontal distance was derived in formula (16). By selecting a maximum slope of 25% and a total horizontal distance of 400 m, a proportional diagram of horizontal and vertical distances was generated, as shown in Fig. 3, which visually displayed the terrain characteristics of the actual test site.

$$y = \begin{cases} \dfrac{m}{2r}x^2 & (0 \leqslant x < r) \\ -\dfrac{m}{2r}\left[(x-2r)^2 + (2r)^2\right] & (r \leqslant x < 3r) \\ \dfrac{m}{2r}(x-4r)^2 & (3r \leqslant x \leqslant 4r) \end{cases} \tag{16}$$

where y—— vertical height, m

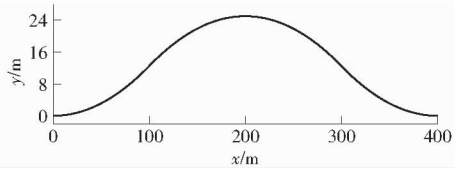

Fig. 3 Curve of test road

To build a realistic simulation system, this study used the CarSim dynamics model with detailed configurations. CarSim offered a variety of preset options for configuring vehicles and their components, allowing flexible adjustments based on different vehicle types and operational requirements. In this study, most of the physical characteristics of the vehicle body were configured using the built-in tractor preset model in CarSim. The key parameters of this model were as follows: the sprung mass was 3 500 kg, its dimensions were 4 600 mm in length, 2 100 mm in width and 2 800 mm in height. The powertrain selected had a maximum output of 150 kW, the braking system's front and rear wheel braidking moments were 100 N·m/MPa and 250 N·m/MPa, respectively.

To determine the relationship between the gravitational component, the conventional resistance within operational resistance and the throttle opening, the vehicle started from an initial speed of 0 km/h at a horizontal distance of 0. The throttle opening was gradually increased, allowing the vehicle to accelerate progressively. The Simulink model of this process was shown in Fig. 4. When the vehicle reached a quarter of the total horizontal distance, the terrain slope gradually increased from 0 to its maximum value, and the data for the vehicle's pitch angle and throttle opening were recorded during this process. Since the collected data showed slight fluctuations, as indicated by the dashed line in Fig. 5, a cubic polynomial was used to fit the original data, providing a smoother and more stable throttle opening output. The fitted curve was shown as a solid line in Fig. 5.

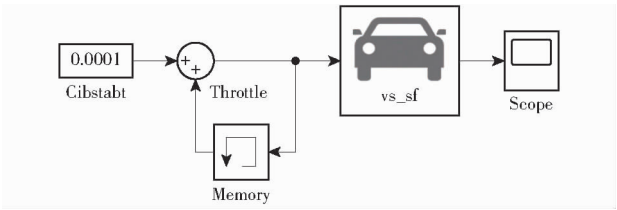

Fig. 4 Measurement model of the relationship between gradient and throttle opening

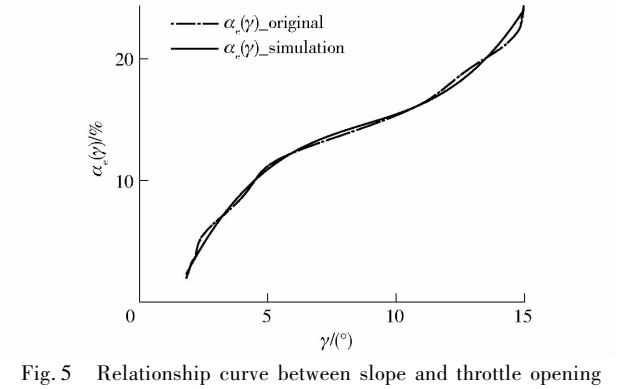

Fig. 5 Relationship curve between slope and throttle opening

Since static friction was typically greater than sliding friction, to determine the relationship between the gravitational component, the conventional resistance within operational resistance, and the brake master cylinder pressure, the vehicle begins moving at

a certain speed when it reached three-quarters of the total horizontal distance on the test road, and a specific brake master cylinder pressure was applied. Closed-loop PID control was used to adjust the brake master cylinder pressure, allowing the vehicle to maintain a near-constant speed. The Simulink model of this process was shown in Fig. 6. Similarly, a cubic polynomial was used to fit the relationship between brake master cylinder pressure and pitch, and this mapping relationship was shown in Fig. 7.

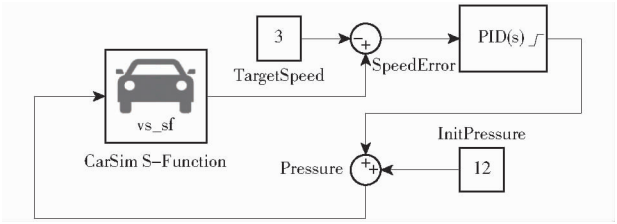

Fig. 6　Measurement model of the relationship between gradient and brake master cylinder pressure

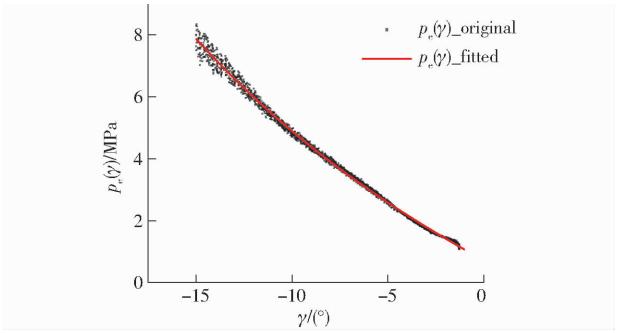

Fig. 7　Relationship curve between gradient and brake master cylinder pressure in CarSim

Based on the relationship between throttle opening and vehicle pitch angle, combined with the PID controller, the throttle opening control system described in formula (13) can be implemented. Its Simulink model was shown in Fig. 8, where the α_e calculation module was an instance of formula (6), and the α_{ne} calculation module was an instance of formula (11). Similarly, the brake master cylinder pressure control system described in formula (14) was established, and its Simulink model was shown in Fig. 9, where the p_e calculation module was an instance of formula (7), and the p_{ne} calculation module was an instance of formula (12).

By combining the throttle opening control system and the brake master cylinder pressure control system, the overall speed control system was established. Its Simulink model was shown in Fig. 10.

1.4　Real-world verification via vehicle chassis

To validate the effectiveness of the hybrid

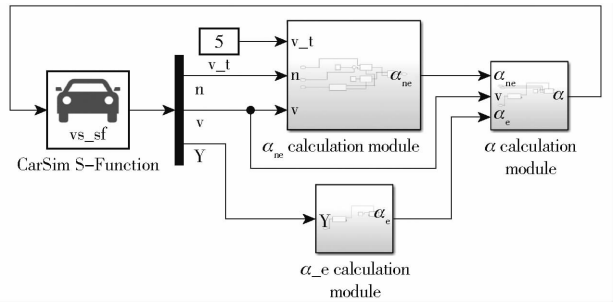

Fig. 8　Throttle valve opening control system

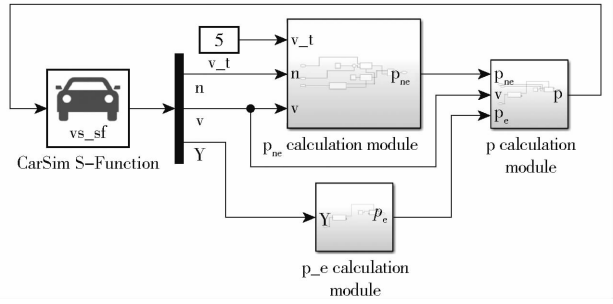

Fig. 9　Brake master cylinder pressure control system

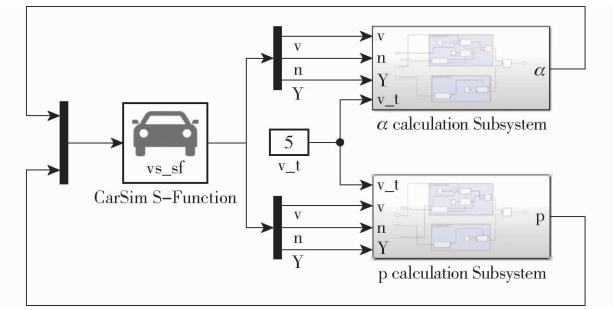

Fig. 10　Speed control system

controller in a real-world environment, simulation experiments were conducted based on the PIX − HOOKE3.0 electric steer-by-wire chassis (PIX). The total weight of the chassis was approximately 600 kg, with a track width of 1 465 mm and a wheelbase of 1 900 mm. The maximum power output was 15.2 kW, with a maximum climbing grade of 30% (corresponding to a vehicle pitch angle of approximately 16.7°). The CAN2.0 bus operated at a communication rate of 500 kb/s, with a response frequency of approximately 200 ms. The maximum braking torque was 2.3 N·m, and the control precision was 0.1 MPa.

To obtain the vehicle's attitude, a Newton − M2 onboard satellite/inertial hybrid navigation system was used. The system provided real-time attitude accuracy of 0.2° (real-time 1σ) and 0.05° (post-processing), with a range of ±120(°)/s. The zero bias stability was <10(°)/h (Allan Variance) and <30(°)/h (10 s average, 1σ).

As shown in the Fig. 5, Fig. 11, the mapping relationship between throttle opening and pitch angle shared a consistent overall trend, but their curve shapep different.

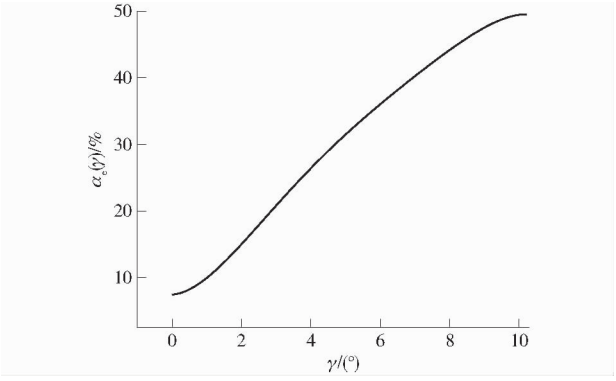

Fig. 11 Relationship curve between pitch and throttle opening in real-world conditions

The core reason lay in the power system type. The CarSim simulation used a fuel engine model, where the relationship between throttle opening and driving force was affected by fuel injection, intake efficiency, combustion conditions and transmission mechanical losses, resulting in nonlinear characteristics. The PIX real vehicle used an electric motor, whose power output was directly controlled by current. The relationship between current and torque the core source of driving force was more stable and linear, leading to differences in their throttle opening mapping curves.

The braking system differs. Both CarSim simulation and PIX real vehicle followed the same principle: applying force to the brake pads, which converted to braking force. With no complex nonlinear interference, as shown in the Fig. 7, Fig. 12, braking-related mapping curves showed linear characteristics.

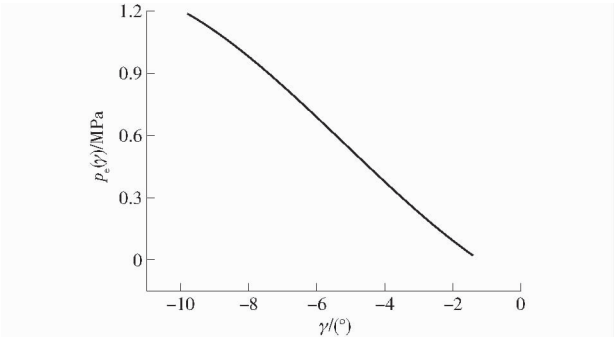

Fig. 12 The relationship curve between pitch and brake pressure in real-world conditions

The experimental site was chosen as a section of sloped terrain on the east campus of China Agricultural University. The experimental environment was shown in Fig. 13. The maximum slope of the terrain was 9.46°.

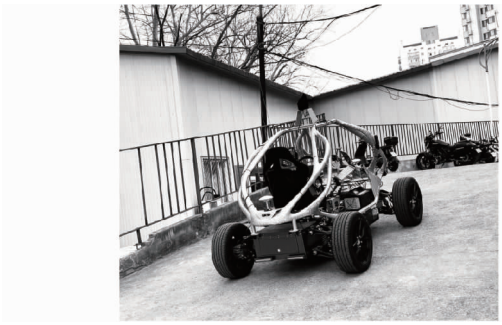

Fig. 13 Environmental conditions of the experimental site

2 Results and discussion

The slope of typical sloping farmland was usually less than 25%. Farmland with slopes exceeding this value were unsuitable for cultivation due to issues such as soil erosion[22-23]. Therefore, in the simulation experiments, the maximum slope was set to 25%. Additionally, the operating speed of agricultural machinery typically ranged from 4 ~ 10 km/h[24-25]. Based on this, the target speeds of 5 km/h, 7 km/h, and 9 km/h were selected.

After setting the above data, the vehicle started from the origin. During the experiment, data on the vehicle's speed, longitudinal position, horizontal position, throttle opening, and brake master cylinder pressure were recorded. Furthermore, a control model using only the PID controller was established for comparison. The PID parameters were tuned, and comparative experiments were conducted under the same conditions, with relevant data recorded throughout the test process.

To evaluate the performance of the proposed speed control method based on ground slope combined with the PID controller (GS + PID), a comparison was made with the method using only the PID controller, and several key indicators were calculated. The results were shown in Table 1. RMSE was used to assess the overall deviation of the controller from the target speed throughout the entire operation, being particularly sensitive to larger errors. MAE measured the average error produced by the system during the entire operation, treating each error value equally without amplifying larger errors like RMSE did. MAPE evaluated the percentage error relative to the actual value, making it unit-independent and suitable for

Table 1　Performance comparison of GS + PID and PID controllers

Data indicator	Method	5 km/h			7 km/h			9 km/h		
		Uphill	Downhill	Overall	Uphill	Downhill	Overall	Uphill	Downhill	Overall
RMSE/(km·h^{-1})	PID	0.61	1.01	0.83	1.02	1.62	1.35	1.45	1.99	1.73
	GS + PID	0.12	0.11	0.11	0.15	0.13	0.14	0.21	0.11	0.17
MAE/(km·h^{-1})	PID	0.42	0.97	0.69	0.69	1.51	1.09	1.04	1.85	1.43
	GS + PID	0.06	0.09	0.08	0.07	0.11	0.09	0.11	0.10	0.11
MAPE/%	PID	8.53	19.45	13.84	9.95	21.65	15.63	11.59	20.63	15.96
	GS + PID	1.34	1.88	1.61	1.13	1.60	1.36	1.27	1.15	1.21
PE/(km·h^{-1})	PID	2.16	1.53	2.16	3.64	2.85	3.64	4.36	2.90	4.36
	GS + PID	0.45	0.35	0.45	0.55	0.30	0.55	0.72	0.33	0.72

comparison across different speed ranges. PE was used to measure the maximum error that occurred during the system's operation, reflecting the control system's performance under extreme conditions.

For the Case DV series precision seeder, the required seeding speed was 6 ~ 8 km/h, with a central speed of 7 km/h. Taking 7 km/h as an example, the statistical analysis of the data in Table 1 demonstrated that the GS + PID speed controller outperformed the PID-only controller across all road sections. Specifically, the GS + PID controller reduced the RMSE on both uphill and downhill sections, with the error decreasing from 1.62 km/h (PID controller) to 0.13 km/h on downhill sections. This indicated improved speed control accuracy during slope changes. Furthermore, the GS + PID controller achieved lower MAE and MAPE values (e.g., the total road section error decreases from 15.63% to 1.36%), reflecting better stability under varying conditions. In particular, the PID controller tended to produce larger errors on downhill sections, whereas the GS + PID controller, with its more precise feedback mechanisms, minimized errors and speed fluctuations. The reduced PE further illustrated the GS + PID controller's ability to handle larger speed fluctuations, ensuring smoother operation of agricultural machinery on uneven terrain. Overall, the GS + PID speed controller demonstrated superior speed stability, disturbance resistance and robustness.

In the field tests, four sets of experiments were conducted: the PIX built-in speed controller for uphill and downhill, the GS + PID speed controller for uphill and downhill. In these experiments, the response frequency of the chassis control system was 5 Hz, the chassis information feedback frequency was 10 Hz, and the pitch angle update frequency was 50 Hz. All tests started from a flat surface with an initial speed of 7 km/h. The slope, throttle, brake and vehicle speed data were recorded and plotted over time during the tests.

In the uphill test, with a target speed of 7 km/h, the velocity profiles obtained using the GS + PID speed controller and the PIX built-in speed controller were shown in Fig. 14. It can be seen that the GS + PID speed controller was more stable than the PIX built-in speed controller. During the uphill test, the GS + PID speed controller more precisely maintained the target speed, effectively mitigating speed fluctuations caused by external disturbances or changes in slope. In contrast, the PIX built-in controller exhibited larger speed deviations at certain points, demonstrating lower stability. The speed of PIX ranged from a minimum of 2 km/h to a maximum of 14 km/h.

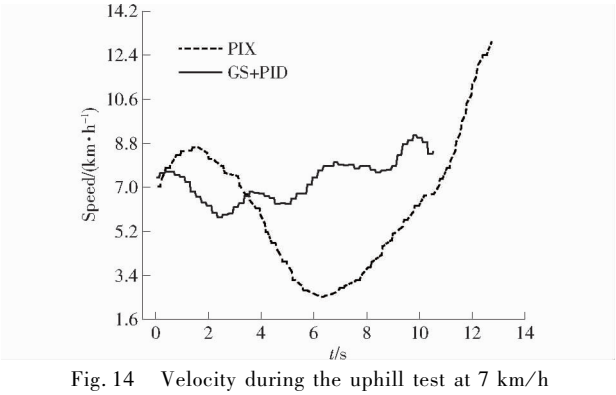

Fig. 14　Velocity during the uphill test at 7 km/h

The curves of throttle opening and pitch variation over time during the operation of the GS + PID speed controller were plotted on the same graph, as shown in Fig. 15. It can be observed that the throttle opening was mainly influenced by changes in slope, but it did not exactly follow the slope variation. This was because the PID controller adjusted the throttle opening appropriately during operation to meet the varying

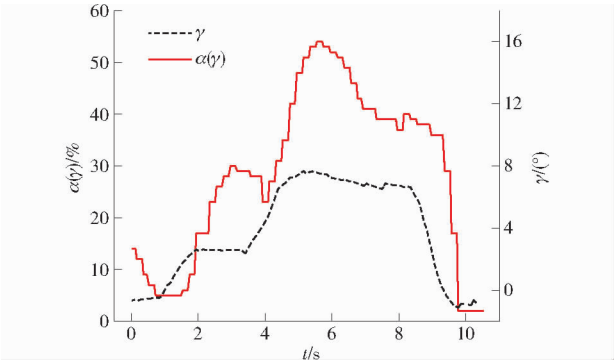

Fig. 15 Throttle opening and pitch variation over time during the operation of the hybrid controller

driving demands caused by changes in slope.

Similarly, in the downhill test, with a target speed of 7 km/h, the velocity profiles obtained using the GS + PID speed controller and the PIX built-in speed controller were shown in Fig. 16. It can be observed that the GS + PID speed controller maintains better speed control, more steadily keeping the target speed during the descent. In contrast, the built-in controller of the PIX system experiences significant speed fluctuations, with speeds dropping below 4 km/h and rising above 14 km/h.

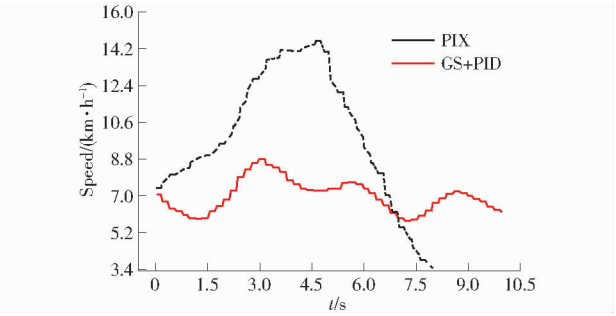

Fig. 16 Velocity profiles during the downhill test at 7 km/h

Fig. 17 showed the relationship between brake pressure and slope variation over time during the operation of the GS + PID speed controller. Similar to Fig. 15, it can be observed that brake pressure was primarily influenced by changes in slope. The PID

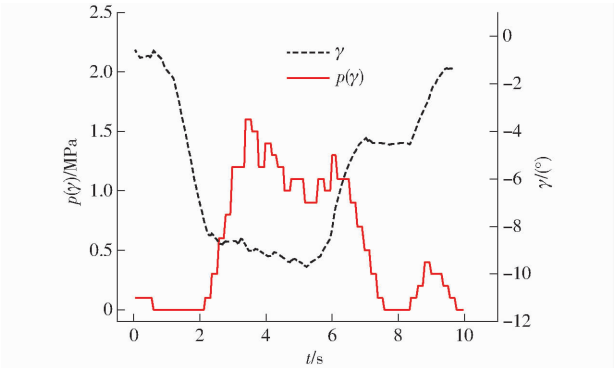

Fig. 17 Brake pressure and pitch variation over time during the operation of the hybrid controller

controller dynamically adjusted the brake pressure based on different slope conditions during operation, ensuring stable vehicle performance across varying slopes.

The specific data in Table 2 showed that the GS + PID speed controller outperformed the PIX built-in speed controller in all indicators during both uphill and downhill phases. In terms of RMSE, the GS + PID speed controller achieved values of 0.54 km/h during uphill and 0.47 km/h during downhill, far lower than the 2.75 km/h and 4.37 km/h recorded for the PIX controller, indicating superior speed control accuracy. Similarly, the MAE results highlighted the advantages of the GS + PID speed controller, with average errors of 0.46 km/h uphill and 0.39 km/h downhill, compared to 2.24 km/h and 3.69 km/h for the PIX built-in speed controller, demonstrating smaller errors throughout the operation.

Table 2 Comparison of speed control performance indicators for different control methods during uphill and downhill phases

Data indicator	Method	Uphill	Downhill
RMSE/(km·h⁻¹)	GS + PID	0.54	0.47
	PIX	2.75	4.37
MAE/(km·h⁻¹)	GS + PID	0.46	0.39
	PIX	2.24	3.69
MAPE/%	GS + PID	6.48	5.43
	PIX	31.22	51.28
PE/(km·h⁻¹)	GS + PID	1.27	1.07
	PIX	5.94	7.59

The MAPE data further illustrated this improvement, with relative errors of 6.48% during uphill and 5.43% during downhill for the GS + PID speed controller, while the PIX built-in speed controller exhibited higher errors of 31.22% and 51.28%, respectively, reflecting enhanced control stability. Moreover, for the PE indicator, the GS + PID speed controller achieved maximum errors of 1.27 km/h uphill and 1.07 km/h downhill, much lower than the 5.94 km/h and 7.59 km/h of the PIX built-in speed controller, showcasing stronger anti-fluctuation capability and robustness.

In summary, the GS + PID speed controller demonstrated clear advantages over the PIX built-in speed controller in terms of speed control accuracy, stability, and anti-interference performance. Particularly in

complex terrain with significant slope variations, the GS + PID speed controller better maintained the target speed, reduced speed fluctuations, and enhanced overall control performance.

3 Conclusion

(1) A hybrid speed control method that combined a ground slope-based controller with a PID controller was proposed to address the speed stability challenges of unmanned agricultural machinery operating on sloped farmland. By establishing the relationships between pitch angle, throttle opening, and brake master cylinder pressure, and integrating these with the PID controller, the system dynamically adjusted control outputs to achieve precise speed regulation under varying slope conditions.

(2) Simulation and real-world test results demonstrated the advantages of this method in terms of control accuracy, stability, and disturbance resistance when compared with traditional controllers. For example, in field tests, the RMSE of the GS + PID controller was 0.54 km/h, while that of the PIX controller was 2.75 km/h.

(3) The RMSE of the field test for uphill conditions was 0.54 km/h, which was slightly higher than the 0.15 km/h RMSE of the simulation due to terrain differences. However, both follow low-error speed stabilization. This showed that the hybrid speed controller's performance on sloped terrains aligned closely with simulation results, further confirming its reliability and practical value in actual agricultural applications.

References

[1] LAN Y, ZHAO D, ZHANG Y, et al. Exploration and development prospect of eco-unmanned farm modes[J]. Transactions of the CSAE, 2021, 37(9): 312 – 327. (in Chinese)

[2] YIN Y, MENG Z, ZHAO C, et al. State-of-the-art and prospect of research on key technical for unmanned farms of field corp [J]. Smart Agriculture, 2022, 4(4): 1 – 25. (in Chinese)

[3] CHEN W, ZHU J, CHEN X, et al. The current situation of the development of agricultural mechanization of slope farmland in our country[J]. Journal of Agricultural Mechanization Research, 2017, 39(5): 1 – 5,11. (in Chinese)

[4] YANG L, YAN B, ZHANG D, et al. Research progress on precision planting pechnology of maize[J]. Transactions of the Chinese Society for Agricultural Machinery, 2016, 47(11): 38 – 48. (in Chinese)

[5] WANG X, ZHAO C, MENG Z, et al. Design and experiment of variable rate fertilizer applicator[J]. Transactions of the CSAE, 2004,20(5): 114 – 117. (in Chinese)

[6] XIE C, ZHANG D, YANG L, et al. Experimental analysis on the variation law of sensor monitoring accuracy under different seeding speed and seeding spacing[J]. Computers and Electronics in Agriculture, 2021, 189: 106369.

[7] WANG Zhuo, LIU Zhixiang, BAI Xiaoping, et al. Longitudinal acceleration tracking control of tractor cruise system[J]. Transactions of the Chinese Society for Agricultural Machinery, 2018, 49(1):21 – 28. (in Chinese)

[8] LIANG Y, DONG H, LI D, et al. Adaptive eco-cruising control for connected electric vehicles considering a dynamic preceding vehicle[J]. E-Transportation, 2024, 19: 100299.

[9] OLEIWI B K, MOHAMED M J. Optimal design of linear and nonlinear PID controllers for speed control of an electric vehicle [J]. Journal of Intelligent Systems, 2024, 33(1): 11 – 85.

[10] KAYACAN E, KAYACAN E, RAMON H, et al. Towards ag-robots: trajectory control of an autonomous tractor using type-2 fuzzy logic controllers[J]. IEEE-ASME Transactions on Mechatronics, 2014, 20(1): 287 – 298.

[11] ZHAO C, WEI C, FU W, et al. Design and experiment of cruise control system for hydrostatic transmission tractor[J]. Transactions of the Chinese Society for Agricultural Machinery, 2021, 52(4): 359 – 365. (in Chinese)

[12] WU C, GAO X, WU S, et al. Feedforward stabilized speed control of driverless tractor based on DEM[J]. Transactions of the CSAE, 2024, 40(10): 24 – 31. (in Chinese)

[13] XIONG Lu, CHEN Chen, FENG Yuan. Modeling of distributed drive electric vehicle based on co-simulation of Carsim/ Simulink[J]. Joural of System Simulation, 2014,26(5):1143 – 1148,1155. (in Chinese)

[14] YANG Z. Research and development of the electronic throttle control system based on fuzzy-PID[D]. Changsha: Hunan University, 2009. (in Chinese)

[15] XIE H, LIU S. Lateral and longitudinal motion control of unmanned vehicles using model predictive control[J]. Journal of Automotive Safety and Energy, 2019, 10(3): 326 – 333.

[16] XI Y, LI W, LIN S. Model predictive control-status and challenges[J]. Acta Automatica Sinica, 2013, 39(3): 222 – 236.

[17] Editorial Department of China Journal of Highway and Transport. Review on China's automotive engineering research progress: 2017[J]. China Journal of Highway and Transport, 2017, 30(6): 1 – 197. (in Chinese)

[18] ZHAO Shengchao, ZHU Lijing. Cruise control system based on joint simulation of CarSim and Simulink[J]. Open Access

Library Journal, 2018, 5(7): 1 - 8.
[19] ZHU B, ZHANG P, ZHAO J, et al. Review of scenario based virtual validation methods for automated vehicles[J]. China Journal of Highway and Transport, 2019, 32(6): 1 - 19. (in Chinese)
[20] LI Z. Modeling, simulation and analysis of automotive handling and stability based on CarSim[D]. Changchun: Jilin University, 2007. (in Chinese)
[21] XIONG L, CHEN C, FENG Y. Modeling of distributed drive electric vehicle based on co-simulation of Carsim/Simulink[J]. Journal of System Simulation, 2014, 26(5): 1143 - 1148, 1155.
[22] WEI S, ZHANG Y, LIU B, et al. Spatial distribution characteristics of soil physical properties of sloping cultivated land with ridges in the black soil region of northeast China[J]. Journal of Soil and Water Conservation, 2024, 31(4): 135 - 144.
[23] TU Anguo, XIE Songhua, YU Zhongbo, et al. Long-term effect of soil and water conservation measures on runoff, sediment and their relatio/nship in an orchard on sloping red soil of southern China[J]. Public Library of Science, 2018, 13(9): 1 - 19.
[24] LUO X, LIAO J, HU L, et al. Improving agricultural mechanization level to promote agricultural sustainable development[J]. Transactions of the CSAE, 2016, 32(1): 1 - 11. (in Chinese)
[25] HE J, LI H, CHEN H, et al. Research progress of conservation tillage technology and machine[J]. Transactions of the Chinese Society for Agricultural Machinery, 2018, 49(4): 1 - 19. (in Chinese)

基于坡度和 PID 混合控制方法的坡地农机稳速控制方法

吴才聪[1,2] 徐海松[1,2] 高星宇[1,2]
(1. 中国农业大学信息与电气工程学院,北京 100083; 2. 农业农村部农机作业监测与大数据应用重点实验室,北京 100083)

摘要: 农业机械的速度稳定控制可提升作业质量与效率。针对农田坡度变化对无人作业农机速度稳定性的影响,本文提出一种混合控制方法,由坡度控制器与比例-积分-微分(PID)控制器组成混合控制器。农机速度受纵向力影响,包括与坡度相关的常规力和难以估计的滑动摩擦力等。针对常规力设计了坡度控制器;针对滑动摩擦力采用 PID 控制器。通过混合 2 种控制器,可动态调节油门开度与制动总泵压力,确保农机在坡地农田中稳定行驶。在目标速度为 7 km/h 仿真测试中,实现了速度稳定控制,均方根误差 0.11 km/h,平均绝对百分比误差 1.6%。实际试验平台的田间试验结果表明,本方法有效,在不同坡度条件下能稳定控制速度,验证了混合控制器具有更优的控制性能,实现了农机行驶速度的精准控制,能满足农机作业的稳定性要求。

关键词: 农田坡度; PID 控制器; 稳定速度控制; 农业机械; 无人作业

基金项目: 国家重点研发计划项目(2023YFE0208200)